VOL. 1, NO. 2, NOVEMBER 2012 ISSN 2305-493X
ARPN Journal of Earth Sciences

www.arpnjournals.com

DOWNHOLE REFRACTION SURVEY IN NIGER DELTA BASIN: A 3-LAYER MODEL

F. Kolawole, C. Okoro and O. P. Olaleye
Seismology Department, Chinese National Petroleum Corporation, Port-Harcourt, Nigeria
E-Mail: folapoint@yahoo.com evagschris@yahoo.com seun2k32003@yahoo.com

ABSTRACT

Downhole refraction survey was carried out in the Elem-Sangama area of River State, Niger Delta Basin. Data sets from 15 refraction points positioned at 4km grid intervals were processed and interpreted, and results show a 3-layer model for two consecutive points and 2-layer model for the other 13 refraction points. A correlation and analysis of observed lithological successions, velocities and depths of boundaries across the two refraction points suggest an irregularity caused by faulting along the true base of weathering as the possible origin of this event. The method of analysis and resolution for 3-layer models adopted in this study may be used in resolving such cases observed during refraction seismic surveys in the Niger Delta Basin.

Keywords: downhole, seismic refraction, seismic data acquisition, weathering layer, consolidated layer, 3- layer model, Niger Delta Basin.

INTRODUCTION

Geophysical properties of the shallow layers of the earth have been investigated and reported by various workers using field techniques such as uphole, downhole and LVL methods of refraction survey (Telford *et al*., 1990, Enikanselu, 2008). These methods provide information on the velocity and thickness of the weathering layer of the earth as well as the velocity of the underlying consolidated layer. Processing of acquired seismic data requires corrections for variations in elevations on land, source and receiver depths (marine airgun and land source), tidal effects (marine), velocity/thickness of near-surface layers (weathering layers/LVL) and change in data reference times. This is known as static correction (Hatherly *et al*., 1994).

Weathering layer of the substratum refers to the shallow surface layer composed of weathered material such as soil, sand, gravel etc. which are unconsolidated (loose) materials. These layers are often typified by low seismic velocities (hence the common name LVL- low velocity layer). Base of weathering can be described as the boundary between the weathered layer and consolidated layer.

STUDY AREA

The Elem-Sangama area, within which the study was carried out, is located approximately between latitudes 4º 33'N and 4º 46'N and longitudes 6° 26'N and 6° 38'N and is underlain by the sediments of the Niger Delta Basin of southern Nigeria (Figure-1). The area is located southwest of Port-Harcourt city, Rivers State; and it is drained by numerous rivers, creeks and mangrove swamps (Figure-2).

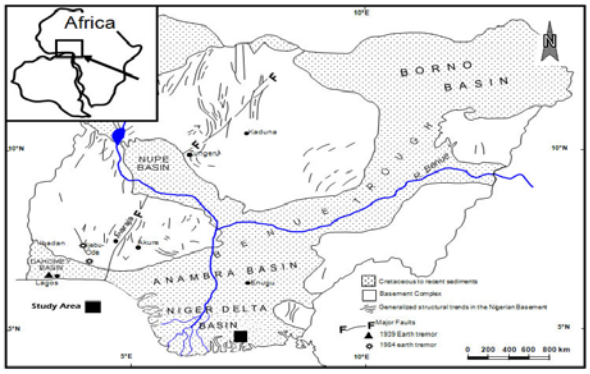

Figure-1. Generalized geologic map of Nigeria showing the study area. (After Odeyemi *et al*., 1999).

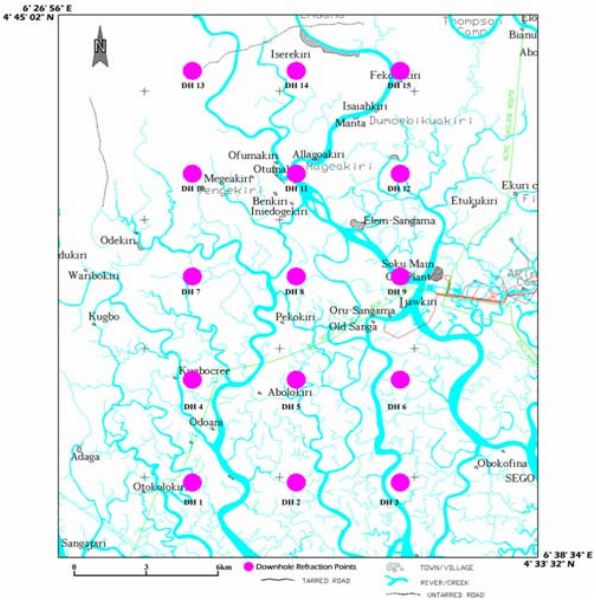

Figure-2. Base map of Elem-Sangama area of Niger Delta Basin showing the downhole refraction points.

The Niger Delta Basin, located on the West African continental margin, covers approximately 211, 000 sq km and developed south-westwards out of the Anambra Basin and the Benue Trough. It is located southeast of the West African shield, bound on the east by the Oban Massif and the Tertiary Cameroon Volcanic Trend and on the west by the Dahomey Basin. On its south lie the South Atlantic seafloor escarpments underlain by the oceanic crust.

The Niger Delta Basin is a coarsening upward regressive sequences of Tertiary sediments that prograded over a passive continental margin sequence of mainly Cretaceous sediments (Stacher, 1995). The emplacement of the basin took place at the site of the triple junction that led to the separation of the African and the South American plates (Wright, 1968).

The Tertiary sediments of the Basin features the basal Akata Formation which is significantly made up of Shale, overlain by the Agbada Formation which consists of intercalations of shale and sandstone lithologies, and the Benin Formation which is made up of continental clastics. Agbada Formation is the main reservoir rock of the basin, while its shale layers as well as those of the underlying Akata formation serves as the source rocks (Evamy and others, 1978, Doust and Omatsola, 1990).

It is intended in this paper to study three-layer-model events observed on refraction data sets acquired at some locations in the Elem-Sangama area of the Niger Delta Basin and propose its possible causes.

THEORY

Two-Layer Model: For a seismic signal traveling from a surface source A to a receiver at D, it is propagated downwards at a certain velocity V_1, and is critically refracted at B and travels at a velocity V_2 along a horizontal interface XY. It is refracted (at C) back to receiver at D at the surface (Figure-3A).

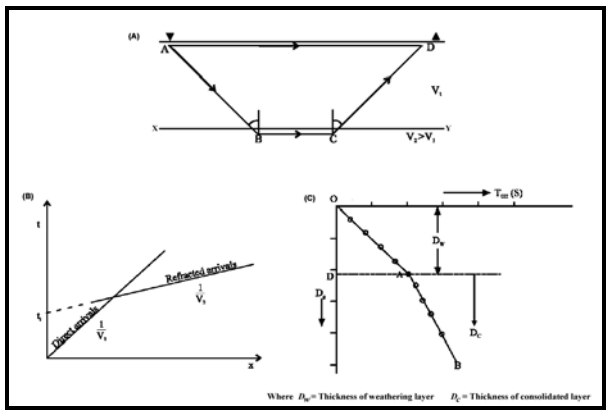

Figure-3. (A) Theoretical ray paths and travel time graph for a 2-layer model. (B) Time-offset relation for a 2-layer model seismic refraction Survey. (C) Time-Depth relation for the Downhole Survey.

Knox (1967) and Dobrin and Savit (1988), calculates travel time T for a two-layer medium in which the energy source is located in the weathering layer:

$$T = \frac{X - 2D_w \tan\theta_c + 2D_c}{V_B} + \frac{2D_w}{V_w \cos\theta_c} \quad (1)$$

Therefore, at X = 0, i.e., at shot point location,

$$T_1 = \frac{2D_w}{\cos\theta_c} \left\{ \frac{1}{V_w} - \frac{-\sin\theta_c}{V_B} \right\} \quad (2)$$

and since, by Snell's law,

$$\theta_c = \arcsin \frac{V_w}{V_B}$$

Then:

$$T_1 = \frac{2D_w \cos\theta_c}{V_w}$$
$$= \frac{2D_w (V_B^2 - V_w^2)^{1/2}}{V_B V_w} \quad (3)$$

Where V_w is the weathering layer velocity; D_w is the thickness of the weathering layer; θ_c is the critical angle of incidence of the wave and T_1 is the intercept time.

An interpretation of the time-depth curve (Figure-3B) shows that the reciprocal of the slope of the lower segment of the curve equals the weathering layer velocity V_w, while that of the upper segment gives the velocity of the underlying consolidated layer, V_c.

Three-layer model

For a three-layer model involving horizontal interfaces, the simple ray path geometry for critical refraction to occur as well as its corresponding travel time-distance graph is shown in Figure-4. As depicted by Figure-4A, the generated signal travels from the source down to the first refractor (at A), where it is refracted into the second medium through to the second interface (at B), at which point it is then critically refracted. From there, the propagating headwave from the lowest refractor travels back from C through the overlying layers to arrive at the receiver at G. Figure-4B shows time-offset relation for a 3-layer model seismic refraction Survey.

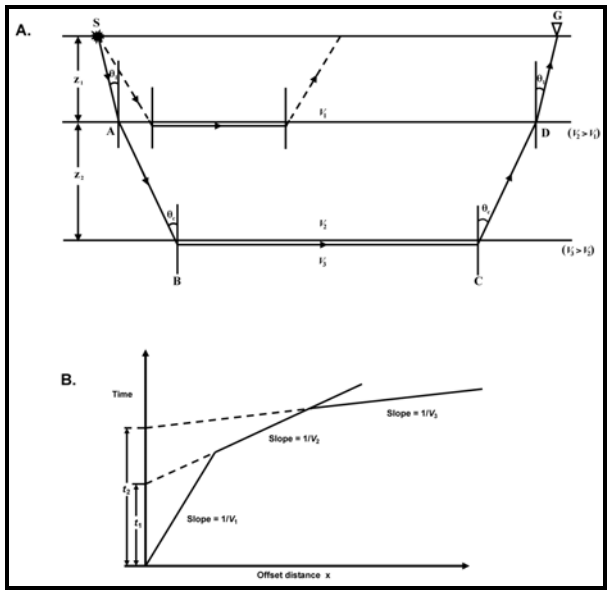

Figure-4. (A) Theoretical ray paths and travel time graph for a 3-layer model. (B) Time-offset relation for a 3-layer model seismic refraction Survey.

Total travel time is:

$$T_{SG} = T_{SA} + T_{AB} + T_{BC} + T_{CD} + T_{DG}$$

Where:

$$T_{SA} = T_{DG} = z_1/V_1 \cos\theta_1$$

$$T_{AB} = T_{CD} = z_1/V_2 \cos\theta_c$$

$$T_{BC} = (x - 2z_1 \tan\theta_1 - 2z_2 \tan\theta_c) / V_3$$

Combining these gives:

$$T_{SG} = x/V_3 + (2z_2 \cos\theta_c)/V_2 - (2z_1 \cos\theta_1)/V_1 \quad (4)$$

$$T_{SG} = x/V_3 + t_2 \quad (5)$$

Where

$$\frac{\sin\theta_1}{V_1} = \frac{\sin\theta_c}{V_2} = \frac{1}{V_3}$$ from Snell's Law

Thickness of refractors is given by:

$$z_1 = t_1 V_1 V_2 / 2(V_2^2 - V_1^2)^{1/2}$$

$$z_2 = t_2 V_2 V_3 / 2(V_3^2 - V_2^2)^{1/2}$$

$$-z_1 V_2 (V_3^2 - V_1^2)^{1/2} / V_1 (V_3^2 - V_2^2)^{1/2}$$

The analysis works by determining V_1, V_2, t_1 and t_2 from the travel time graph for the top two layers, and hence the thicknesses of the first two refractors can be calculated using the equations above.

The downhole method of refraction survey requires a single source on or near the surface, to receivers (sensors) at varying depths in the subsurface (Figure-5). The one-way travel-time is recorded at different depths in order to build up a continuous profile. Recorded one-way travel-times will thereafter be converted to vertical time (T_z) to the surface.

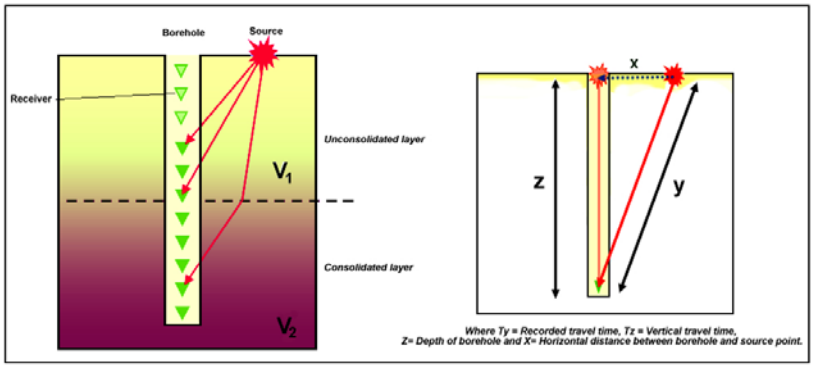

Figure-5. Schematic diagrams describing the theory of downhole seismic survey.

Where T_y = Recorded travel time, T_z = Vertical travel time, Z= Depth of borehole and X= Horizontal distance between borehole and source point.

MATERIALS, METHOD AND DATA PROCESSING

Fifteen (15) 60m-deep bore holes spaced in a 4km grid interval were logged at from the top to the bottom at 0m, 1m, 3m, 5m, 10m, 15m, 20m, 25m, 30m, 40m, 50m and 60m depth levels. Explosive detonator seismic source, hydrophone receiver and Geometrics NZ11 Strata visor Refraction Seismograph equipment were used.

The downhole procedure involves logging a 60m-deep bore hole with a single hydrophone attached to a recording cable and a calibrated rope. The Geometrics NZ11 Strata visor instrument is positioned at the surface and the recording cable is attached to it. During the survey, it was ensured that the hole was filled with water since the receiver in use was hydrophone. Drilling was done with a semi-automated method of drilling in which

5.5' water pump, swivel head, delivery hoses, drill stems (2inches wide and 1.5m long), drill bits (2 and 3 Wings), water-based drilling mud and PVC plastic casings were used. Ditch cuttings were also picked from various depths during drilling. The shots were recorded into 12 recording channels (but only one of the channels was active since only a single hydrophone receiver is involved), while a safe shooting distance of 25m was ensured.

Lab analysis of the first break times from the recorded arriving signals was used to produce a continuous velocity profile between the surface and bottom of the borehole when interpreted with Udysys software. Udysys plots corrected first break times against depths. This is graphically interpreted such that velocities are calculated from the slope of the interpolated lines, while the depth to the base of the weathering layer is solved from the slope breaks or intercepts of the lines (Figure-3C). Fist break listings for all downhole refraction points in the study are shown in Table-1 and interpretation results in Table-2. The distribution of geophysical properties across the study area were analyzed and plotted with Voxler volumetric visualization software package.

Table-1. First-break listing for the 15 downhole refraction points.

DH	Receiver depths (m)											
	0	1	3	5	10	15	20	25	30	40	50	60
	Arrival times for various receiver depths (ms)											
1	7.0	4.0	3.0	4.0	7.0	9.0	12.0	15.0	18.0	24.0	30.0	35.0
2	8.6	4.2	3.0	4.0	6.2	9.8	12.0	16.1	18.1	24.0	30.0	36.6
3	10.1	4.2	2.8	3.4	6.4	9.0	12.6	15.5	18.4	24.0	29.5	33.8
4	7.0	5.0	4.0	4.0	7.0	9.0	12.0	15.0	18.0	24.0	29.0	34.0
5	13.5	7.8	4.0	3.8	6.5	9.5	12.5	14.5	17.5	23.8	29.5	34.1
6	10.8	4.1	2.5	3.4	6.1	8.8	12.1	15.8	19.4	24.4	30.4	35.0
7	16.0	11.0	8.0	10.0	15.0	19.0	22.0	25.0	28.0	34.0	38.0	42.0
8	15.0	11.0	6.5	7.5	12.0	17.5	21.5	25.5	29.9	36.5	41.5	46.2
9	12.1	7.1	3.2	4.2	6.7	9.9	13.1	16.7	19.7	26.1	31.1	37.7
10	11.0	9.0	13.0	12.0	14.0	17.0	20.0	23.0	26.0	31.0	37.0	43.0
11	8.5	4.5	3.5	4.6	7.5	9.5	12.5	15.5	18.5	23.9	29.4	33.5
12	6.0	3.2	2.2	3.2	6.2	8.6	11.8	14.4	17.6	23.6	29.7	35.8
13	6.0	3.0	3.0	4.0	6.0	9.0	12.0	15.0	17.0	23.0	29.0	35.0
14	9.1	4.1	2.5	3.0	6.1	9.1	11.5	13.5	18.1	23.2	29.5	35.1
15	6.8	3.5	2.5	3.5	7.0	9.5	12.5	15.0	18.0	23.0	28.5	34.5

Table-2. Interpretation results for the 15 downhole refraction points.

DH	Elevation (m)	Thickness of weathering layer (m)	Velocity of weathering layer (m/s)	Velocity of consolidated layer (m/s)
1	1.8	4.4	595	1724
2	1.7	4.1	521	1699
3	1.3	4.5	467	1783
4	2.3	3.4	452	1781
5	1.4	4.1	359	1778
6	1.7	4.1	442	1686
7	1.6	8.0	269	2090
8	1.9	9.0	273	2183
9	2.2	4.2	393	1617
10	2.2	4.9	263	1726
11	2.5	4.8	500	1844
12	1.4	3.1	571	1667
13	2.8	3.2	533	1742
14	2.2	4.0	522	1699
15	2.7	5.3	639	1819

DATA INTERPRETATION AND DISCUSSIONS

The T-X plots for first break arrivals of signals as observed at the 15 refraction points are presented in Figures 6A to 6O, and ten of these points show 2-layer model while DH07 and DH08 (Figures 6G and 6H) exhibit a 3-layer model.

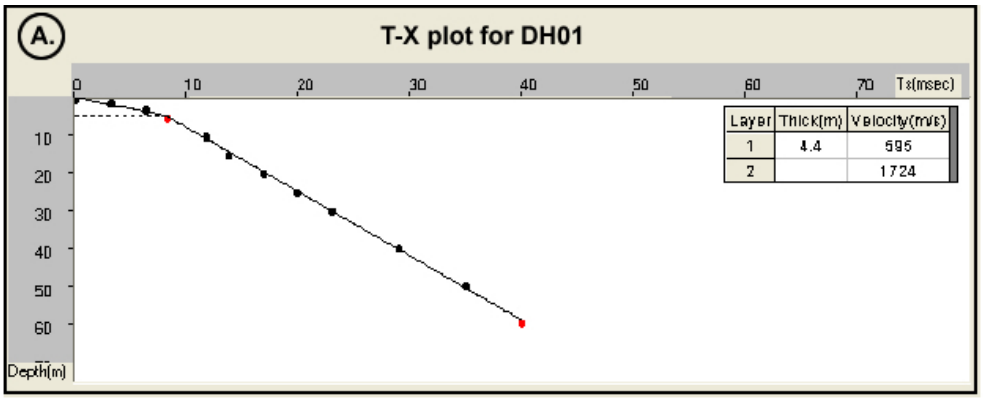

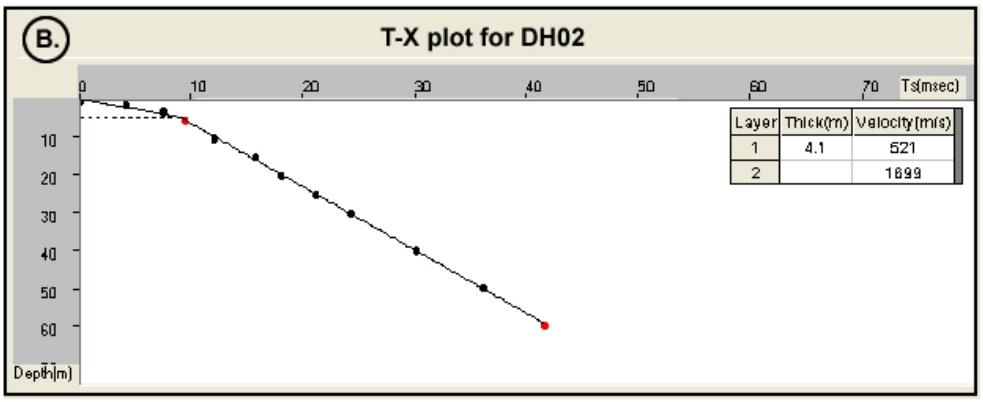

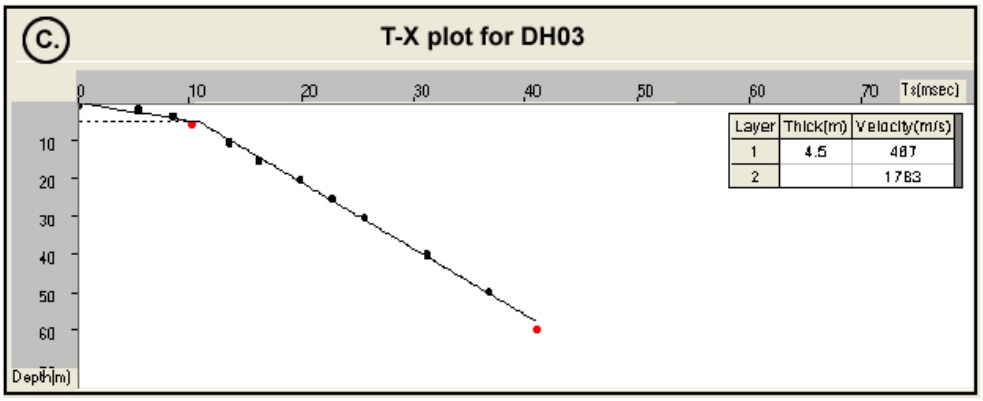

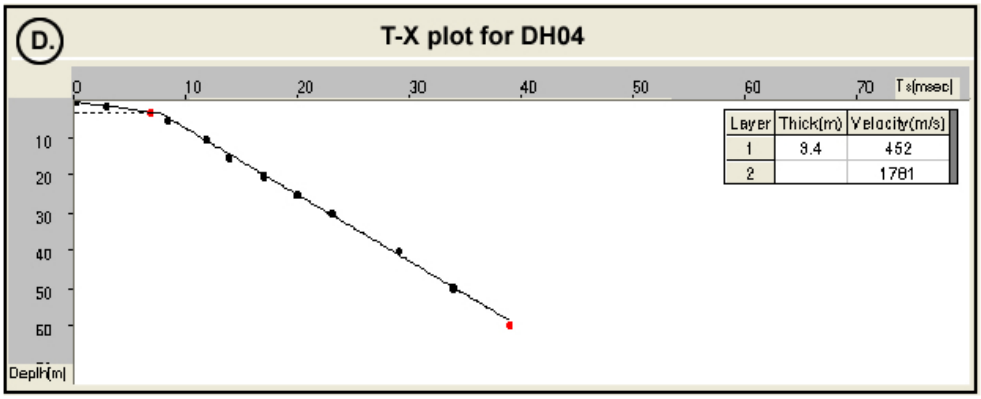

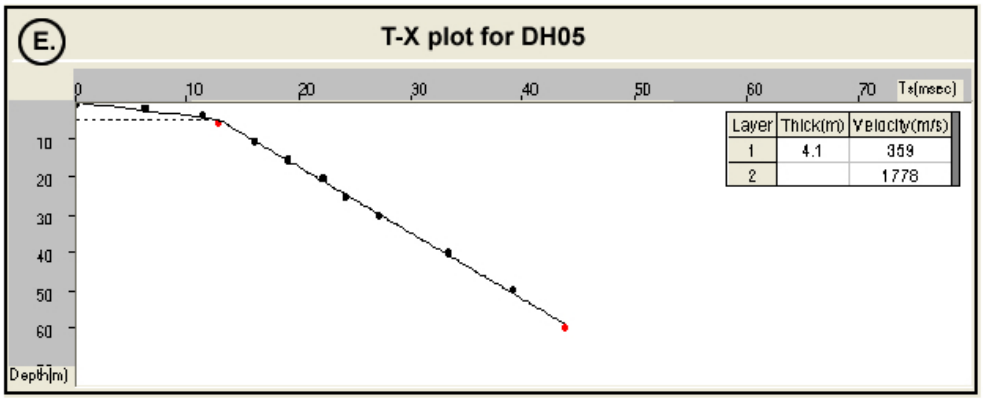

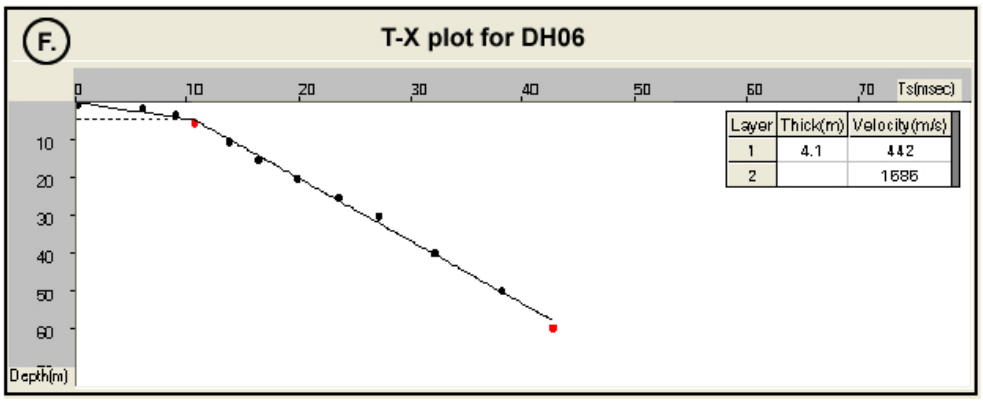

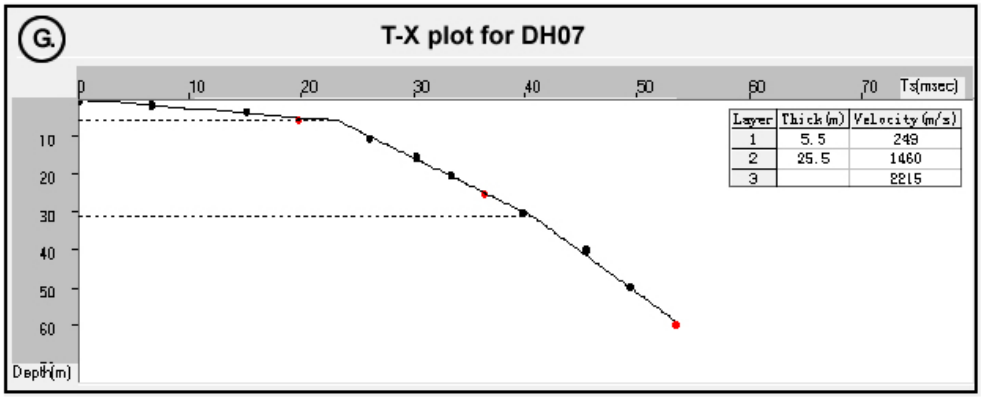

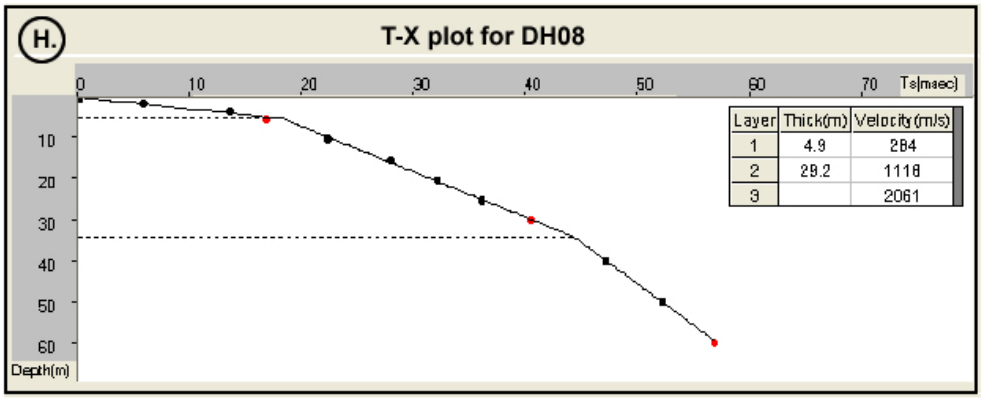

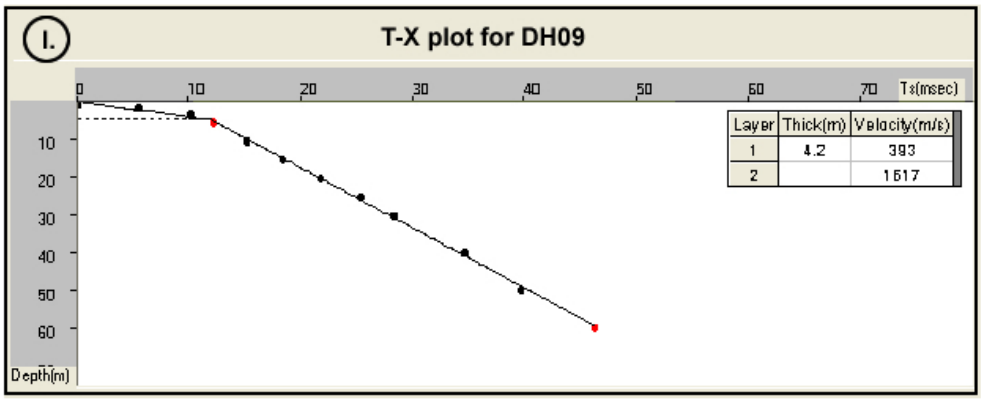

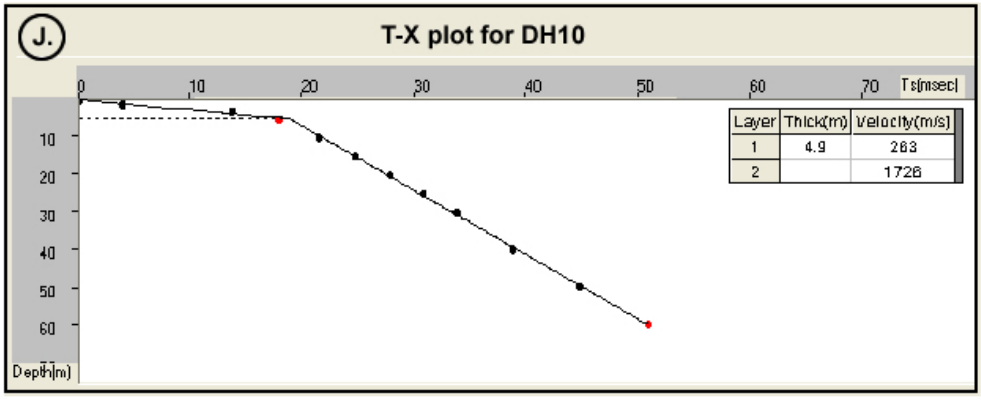

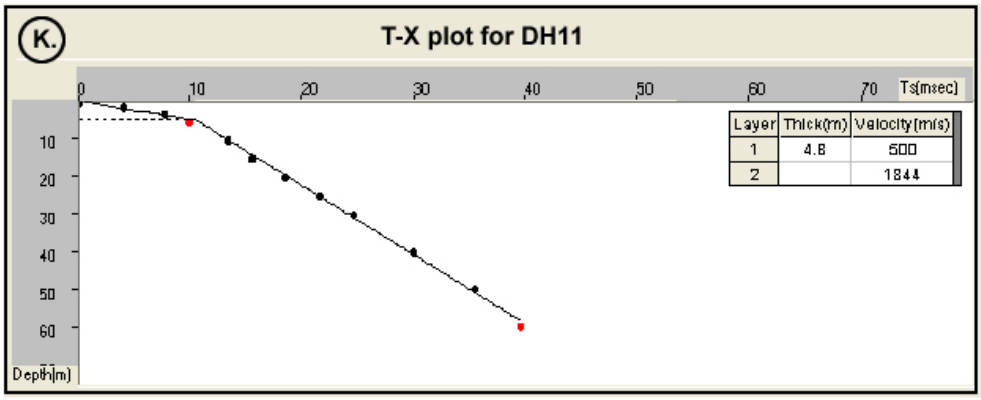

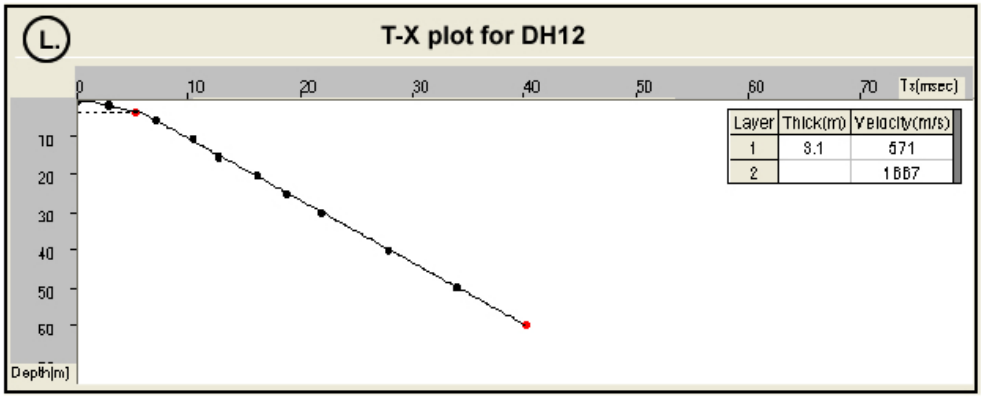

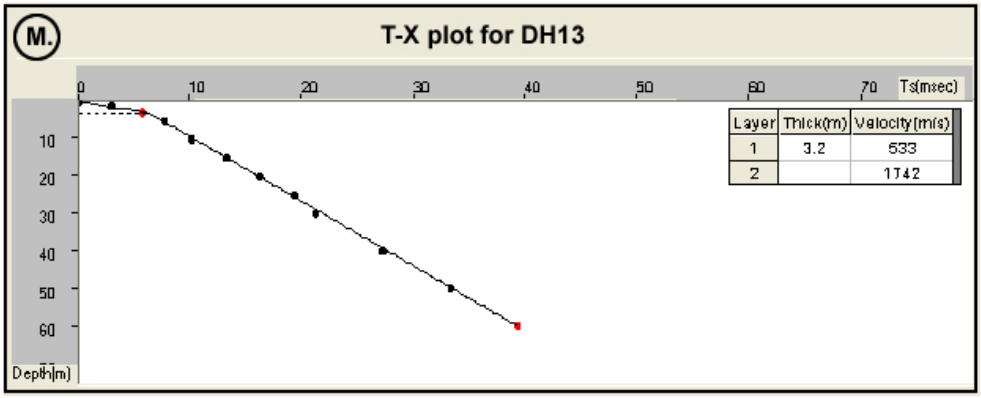

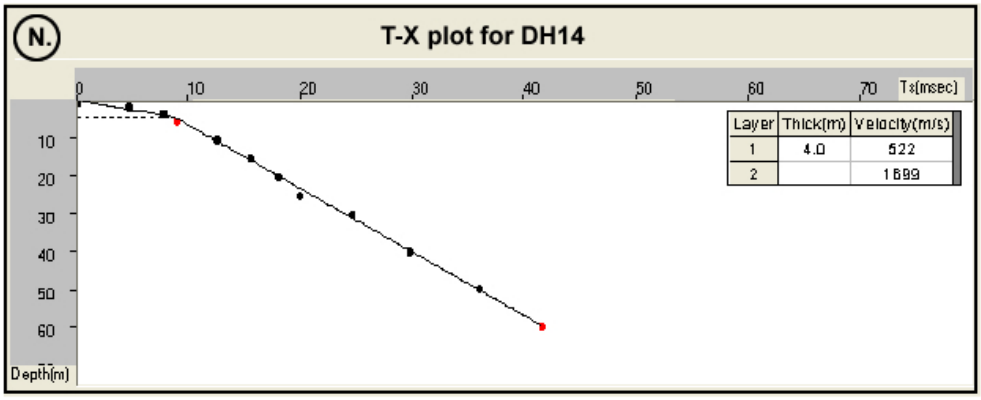

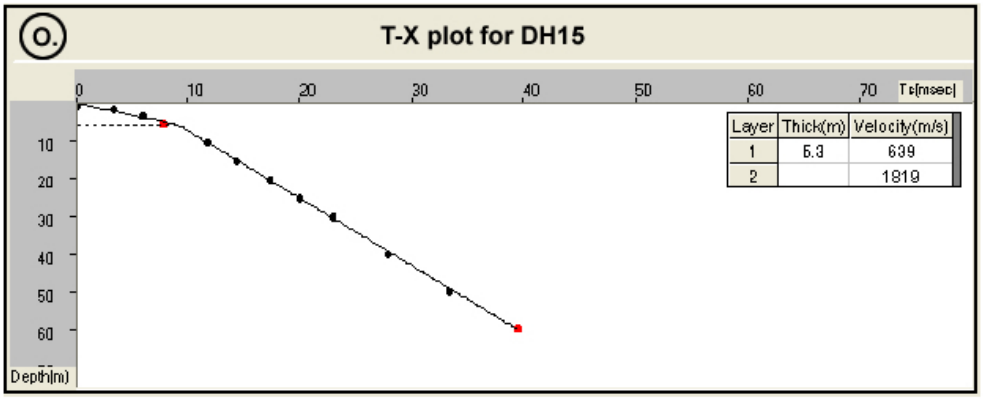

Figure-6A to 6O. T-X plots for all 15 downhole refraction points.

Before any comparison can be made across all the refraction points under study, the observed 3-layer events must first of all be understood and resolved; and while there exits mathematical calculations for a 3-layer model in refraction seismology, the real existence of a layer of intermediate consolidation and velocity within the Niger Delta Basin may not be easily geologically explainable.

A correlation of lithology logs with depths of major deflections along the time-depth curve for both DH07 and DH08 reveals that the 2nd layer occurs at slightly varying depths at both locations as the boundaries are marked at shallower depths at DH08 and at slightly deeper depths at DH07 (on the west). The tie lines for both the base of 1st layer and that of the 2nd layer across DH07 and DH08 appear to lie parallel to each other, both of which apparently conform to the surface topography between the two locations. Also, there is a steep increase in velocities towards the east within the 1st layer (249m/s - 284m/s), which contrasts the trend observed in the two underlying layers (layer 2 and 3) in which velocities increase towards the west (1, 118m/s - 1, 460m/s in the 2nd layer and 2, 061m/s - 2, 215m/s in the 3rd layer). The correlation and observation of lithological successions along the litho-logs of both bore holes (DH07 and DH08)

generally match that of the other bore holes in the study area, and the ubiquitous occurrence of an impervious layer (clay) overlying a porous formation (sand) may preclude an existence of the water Table in the former. It is important to also note that this lithological succession may even demonstrate a type of minor artesian aquifer for the shallow substratal horizons underlying the study area.

This suggests that the 3-layer model observed at these two consecutive refraction points may not be as a result of an occurrence of the water Table at the boundaries even though the slope of the correlation tie lines lies roughly parallel to the topography of the surface. The topography of the water Table within an area reflects the overlying surface relief due to the capillary effect in soils, sediments and other porous media within the area (Freeze and Cherry, 1979). Therefore, an irregularity along the base of weathering may be responsible for the 3-layer-model events observed at the two refraction points in focus. This irregularity may probably originate from an occurrence of faulting within the weathering layer as it has been confirmed that occurrence of faults, 'horst and graben' tectonic, and decay of bed rock can create irregularities along the base of weathering (Thorbecke, 1992).

Nevertheless, an analysis of the distribution of seismic velocities within the 2nd layer (across both DH07 and DH08 bore holes) with the depths of observed major deflections along the time-depth curves may give a clue to the geometry of the irregularity occurring along the true base of weathering. The possibility of existence of a cavity or buried river channel within the weathering layer and stretching across the two bore holes located 4km apart, may not be reasonable since there are no evidences from lithology logs.

Calculating the true thickness and velocity of layers at DH07 and DH08

According to the interpretation of refraction data from both DH07 and DH08 (Figures 6G and 6H), the thick layers of intermediate consolidation and velocity occur at depth intervals between 5.5m and 31m for DH07, and between 4.9m and 34.1m for DH08.

Since there is yet no logical geological condition that can be made to favor the existence of this intermediate layer, and since to an extent, the data set bears a measure of consistency with those from other refraction points surveyed in the area, it is reasonable to resolve to a boundary within the interval. The location of this boundary is found, as shown in Figures-7 and 8, by simply projecting the time-depth curve from above and below the major deflection points to find their intersection (Franklin, 1980). Generally, the results appear to be a little higher than the values from the other refraction points in the study which originally showed 2-layer models.

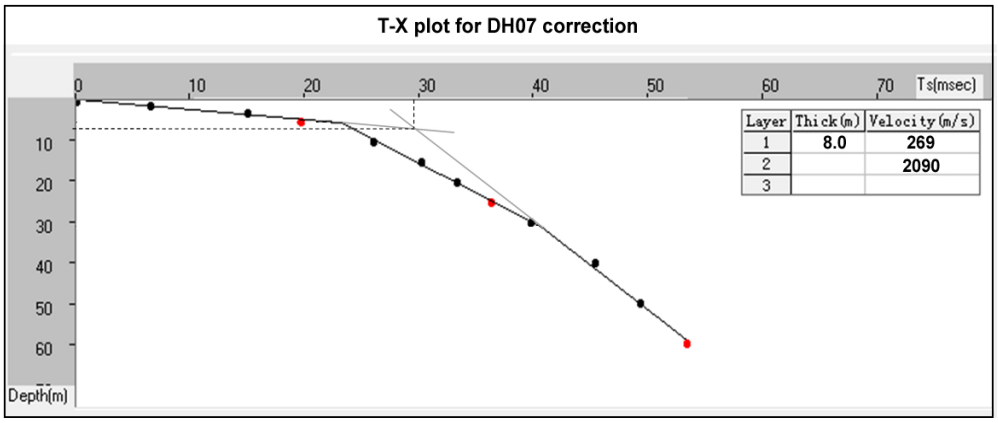

Figure-7. T-X plot for DH07 correction.

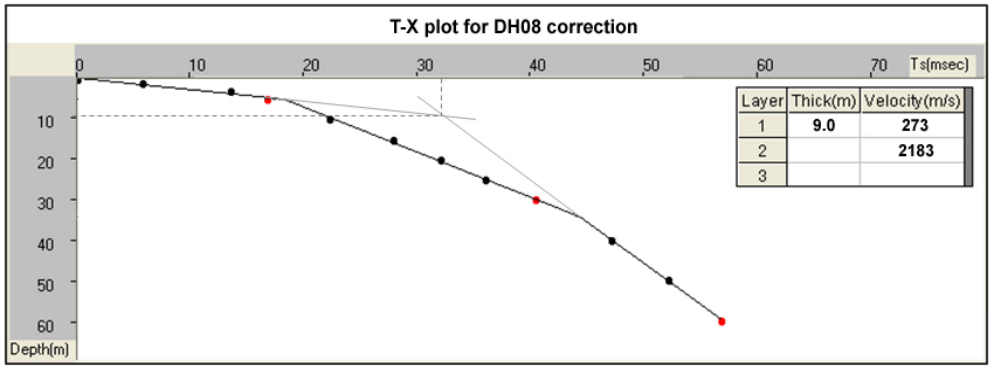

Figure-8. T-X plot for DH08 correction.

For DH07, the interpolation computes a velocity of 269m/s and thickness of 8m for the weathering layer, and a velocity of 2090m/s for the consolidated layer. While for DH08, a thickness of 9m and velocity of 273m/s is estimated for the weathering layer, and 2183m/s for the velocity of the consolidated layer.

Figure-9 explores the relationship between surface elevations of refraction points and the variations in thickness of the weathering layer across the study area. It reveals that weathering thickness generally increases southwards as elevation decreases towards the same direction which creates an E-W-trending margin of intersection of the two planes between DH07-08-09 and DH10-11-12. The non-homogeneity of the earth may explain the inconsistency in the trend at DH04 and DH15. The bulge in weathering thickness at DH07 and DH08 might have been produced by the irregularity along the base of weathering at the two locations. There's also a significant drop in elevation at both DH07 and DH08. Normal faulting in the weathering layer could have resulted in the creation of depression (accommodation) at the surface which allows for more deposition of sediments at the locations thereby significantly increasing the thickness of the weathering layer at these points.

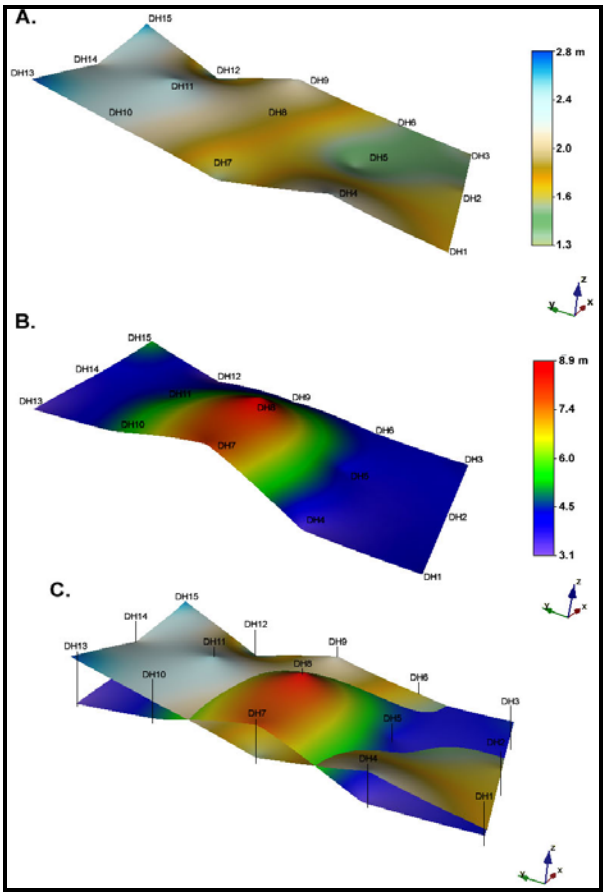

Figure-9. (A) Surface elevation across the study area. (B) Distribution of weathering thickness across the study area. (C) Superimposition of plots A and B.

Figure-10A plots the distribution of weathering thickness across the study area, while Figure-10B plots the same distribution but excludes DH07 and DH08 since their values, being exceptionally higher than others appear to mute the effect of other refraction points with little higher values among the rest. Figure-10C shows an interpolation of the plots 10A and 10B which reveals a strong relationship between DH07, DH08, DH10 and DH11. This relationship can be thought of as in a structural sense.

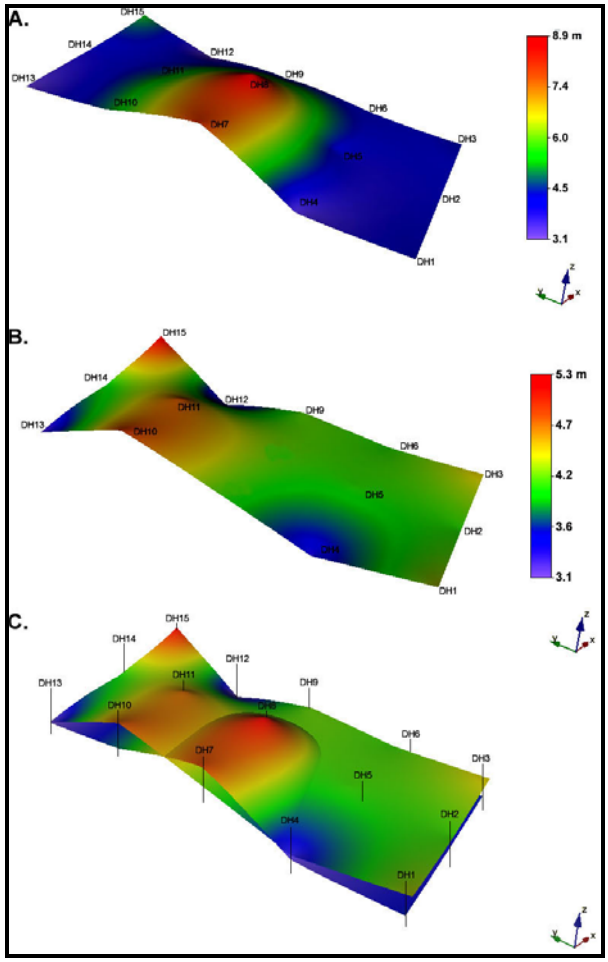

Figure-10. (A) Distribution of weathering thickness across the study area. (B) Distribution of weathering thickness across the study area excluding DH07 and DH08. (C) Superimposition of plots A and B.

The distribution of weathering layer velocity across the study area in comparison with weathering thickness variation is presented in Figure-11. It can be observed that weathering velocity decreases generally towards the south with the most significant drop occurring within the zone of the anomaly (DH07 and DH08) with an extension to DH10 where weathering velocity is lowest. This again confirms another relationship (geophysical in this case) between DH07, DH08 and DH10.

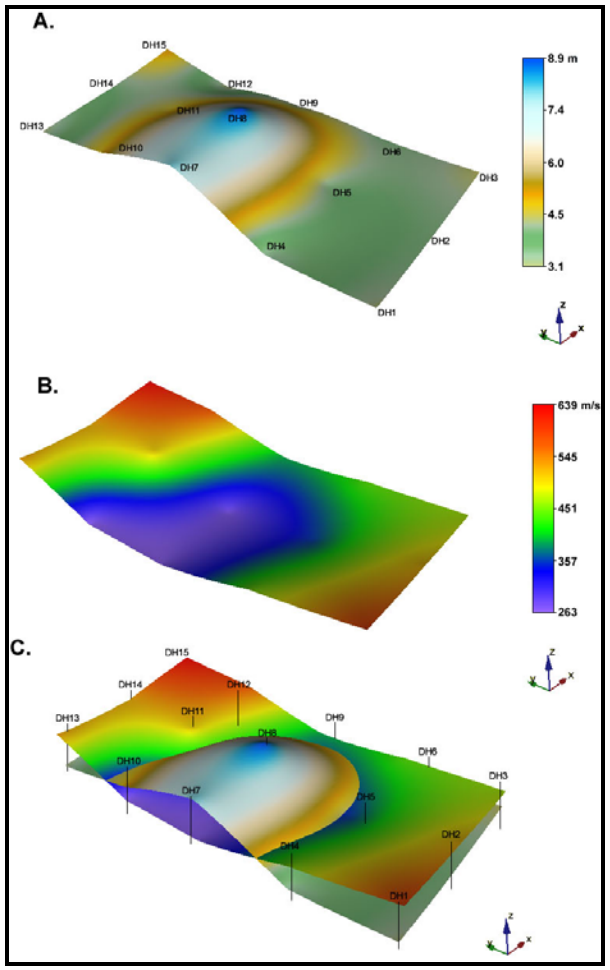

Figure-11. (A) Distribution of weathering thickness across the study area. (B) Distribution of weathering velocity across the study area. (C) Superimposition of plots A and B.

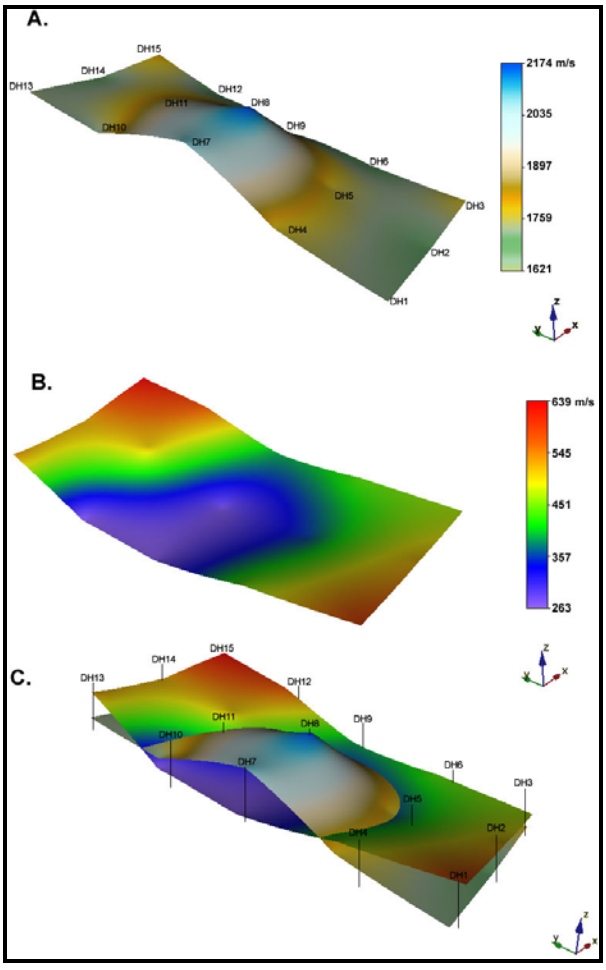

Figure-12. (A) Distribution of velocity within the consolidated layer. (B) Distribution of weathering velocity across the study area. (C) Superimposition of plots A and B.

Seismic velocities within the consolidated layer appear to decrease gradually towards the south but with a sudden and most significant increase at DH07, DH08 and DH11 (Figure-12); which further suggests a northward extension of a substratal geophysical anomaly from DH07 and DH08. It is also interesting to note that the velocity of the consolidated layer is highest at the points where the velocity of the weathering layer is least (DH07 and DH08).

Therefore, strong geophysical and structural relationships occur between DH07, DH08, DH10 and DH11. This is an interesting occurrence since all four points are located in the same region within the study area. It can also be said that DH07 and DH08 are located at the core of the subsurface structure causing the anomaly, while DH10 and DH11 are on its fringes as shown by the variation in thickness and velocity values across both weathering and consolidated layers.

CONCLUSIONS

The correlation and interpretation of observed litho logical successions with velocities and depths of boundaries across the two refraction points with 3-layer models suggest an irregularity along the true base of weathering, probably caused by faulting. It is also clear that the irregular structure extends to the north of these two points as observed in geophysical and structural relationships across all the studied refraction points. The true depths of base of weathering, as well as velocities of

weathering and consolidated layers for the two refraction points with 3-layer models were calculated.

The method of analysis and resolution for 3-layer models adopted in this study may be used in resolving such cases observed during refraction seismic surveys in the Niger Delta Basin.

REFERENCES

Dobrin M. D. and Savit C. H. 1988. Introduction to geophysical prospecting (4th ed). McGraw Hill: New York. 867.

Doust H. and Omatsola E. 1990. Niger Delta, in, Edwards, J. D. and Santogrossi, P.A., eds., Divergent/passive Margin Basins, AAPG Memoir 48: Tulsa, American Association of Petroleum Geologists. pp. 239-248.

Enikanselu P. A. 2008. Geophysical seismic refraction and uphole survey analysis of weathered layer characteristics in the mono field, north western Niger Delta, Nigeria. The Pacific Journal of Science and Technology. 9(2): 537-545.

Evamy B. D., Haremboure J., Kamerling P., Knaap W. A., Molloy F. A. and Rowlands P. H. 1978. Hydrocarbon habitat of Tertiary Niger Delta: American Association of Petroleum Geologists Bulletin. 62: 277-298.

Franklin A. G. 1980. Interpretation of data from uphole refraction surveys: Final Report. U. S. Army Engineer Waterways Experiment Station, Mississippi: 68.

Freeze R. A. and Cherry J. A. 1979. Groundwater. Englewood Cliffs, NJ: Prentice-Hall: 604.

Hatherly P. J., Urosevic M., Lamboure A. and Evans B. J. 1994. A simple approach to calculating refraction statics corrections. Geophys. 59: 156-160.

Knox W. A. 1967. Multilayer near-surface refraction computations. In: Seismic Refraction Prospecting: Musgrave, A. W. (ed.) Soc. Expl. Geophysics. pp. 197-296.

Odeyemi I. B., Anifowose A. Y. B. and Asiwaju-Bello Y. A. 1999. Remote sensing fracture characteristics of Pan African granite batholiths in the Basement Complex of parts of south western Nigeria. The Journal of Techno science. 3: 56-60.

Stacher P. 1995. Present understanding of the Niger Delta hydrocarbon habitat, in: Oti, M.N. and Postma, G. eds. Geology of Deltas; Frotterdam A.A., Bakkema. pp. 57-267.

Telford W. M., Geldart L. P. and Sheriff R. E. 1990. Applied Geophysics. Cambridge University Press: 792.

Thorbecke J. 1992. Weathered layer corrections. DELPHI progress report. Vol. 3, Ch. 4: 115-148.

Uko E. D., Ekine A. S. and Ebeniro J. O. 1992. Weathering Structure of the East-Central Niger Delta, Nigeria. Geophysics. 57(9): 1228-1233.

Wright J. B. 1968. South Atlantic continental drift and the Benue Trough. Tectonophysics. 6: 301-310.